



Arsenic binding to human metallothionein-3†

Cite this: *Chem. Sci.*, 2023, 14, 5756Amelia T. Yuan  and Martin J. Stillman *

All publication charges for this article have been paid for by the Royal Society of Chemistry

Arsenic poisoning is of great concern with respect to its neurological toxicity, which is especially significant for young children. Human exposure to arsenic occurs worldwide from contaminated drinking water. In human physiology, one response to toxic metals is through coordination with the metallochaperone metallothionein (MT). Central nervous system expression of MT isoform 3 (MT3) is thought to be neuroprotective. We report for the first time on the metalation pathways of As^{3+} binding to apo-MT3 under physiological conditions, yielding the absolute binding constants ($\log K_n$, $n = 1-6$) for each sequential As^{3+} binding event: 10.20, 10.02, 9.79, 9.48, 9.06, and 8.31 M^{-1} . We report on the rate of the reaction of As^{3+} with apo-MT3 at pH 3.5 with rate constants (k_n , $n = 1-6$) determined for each sequential As^{3+} binding event: 116.9, 101.2, 85.6, 64.0, 43.9, and 21.0 $\text{M}^{-1} \text{s}^{-1}$. We further characterize the As^{3+} binding pathway to fully metalated $\text{Zn}_7\text{MT3}$ and partially metalated Zn-MT3. As^{3+} binds rapidly with high binding constants under physiological conditions in a noncooperative manner, but is unable to replace the Zn^{2+} in fully-metalated Zn-MT3. As^{3+} binding to partially metalated Zn-MT3 takes place with a rearrangement of the Zn-binding profile. Our work shows that As^{3+} rapidly and efficiently binds to both apo-MT3 and partially metalated Zn-MT3 at physiological pH.

Received 23rd January 2023

Accepted 3rd May 2023

DOI: 10.1039/d3sc00400g

rsc.li/chemical-science

Introduction

Chronic arsenic poisoning of populations has been reported throughout history and continues today. According to the World Health Organization, there are 200 million people exposed to dangerous levels of arsenic from a variety of sources including air, minerals, water, and soil, and most commonly ingested as a component of food or water.^{1,2} Other sources of arsenic include occupational exposure from mining and the electronics industry.¹ Arsenic can be leached into food and water under reducing conditions from surrounding soil and minerals.^{3,4} Arsenic can exist in the inorganic form as $\text{As}(\text{III})$ or $\text{As}(\text{V})$, as well as organic arsenicals of monomethylarsonic acid (MMA), dimethylarsinic acid (DMA), and trimethylarsine oxide.^{3,5} As^{3+} is particularly toxic because of its ability to enter cells and bind to thiol groups of cysteine-containing proteins important in human physiology.^{1,3,5-9}

Chronic and acute arsenic exposure leads to a multitude of symptoms, including abdominal pain, skin lesions, diabetes, neuropathy, hepatic and renal dysfunction, and reproductive consequences.^{3,10} One of the concerns raised is its neurotoxicity, which may lead to developmental adverse outcomes, especially with children.¹¹ This could manifest as epilepsy, lower IQ scores, lower vocabulary scores, higher risk of intellectual disability diagnosis, and lower visuospatial skills, as suggested

by cross-sectional studies ranging from populations in Bangladesh to the United States.¹²⁻¹⁴ While symptoms related to As^{3+} exposure are relatively well-established, the methodology of action is less established. As^{3+} is known to cross the blood-brain barrier, however, its specific target in the neurological system is unknown, with some suggestion of binding to proteins such as the amyloid beta plaques characteristic of Alzheimer's Disease.^{12,13,15} The commonly accepted effect of $\text{As}(\text{III})$, either as inorganic or organic arsenic, is the production of reactive oxygen species.^{1,7,12,14,16,17} These reactive oxygen species then produce downstream effects such as the activation of apoptosis, mitochondrial stress, and neurotransmitter imbalances.^{12,14,15,17}

Metallothioneins (MTs) are cysteine-rich proteins that participate in heavy metal detoxification, as well as homeostatic control of physiologically relevant metals such as Cu^+ and Zn^{2+} .¹⁸⁻²⁰ MTs are found across species, with mammalian MTs classified as 20-cysteinyll proteins ranging from 6–8 kDa in size.²¹⁻²³ Mammalian MTs do not contain any aromatic amino acid residues or disulfide bonds, despite a typical 30% of the sequence being cysteines.²⁴ This family of proteins is thought to participate in the regulation of essential metals by acting as a reservoir and donating these metal ions to apometalloenzymes when necessary.²⁵⁻²⁸ MTs also sequester toxic metals such as Cd^{2+} and As^{3+} that are excreted in the urine or bile.²⁹⁻³² Lastly, MTs are antioxidants in that they can neutralize reactive oxygen species to form disulfide bonds between cysteinyl thiols.³³⁻³⁵ There are four isoforms of mammalian MTs.^{36,37} MT1 and MT2 are inducible by metals and are expressed in all tissues, with primary concentration in the

Department of Chemistry, University of Western Ontario, 1151 Richmond St., London, ON N6A 5B7, Canada. E-mail: martin.stillman@uwo.ca

† Electronic supplementary information (ESI) available. See DOI: <https://doi.org/10.1039/d3sc00400g>



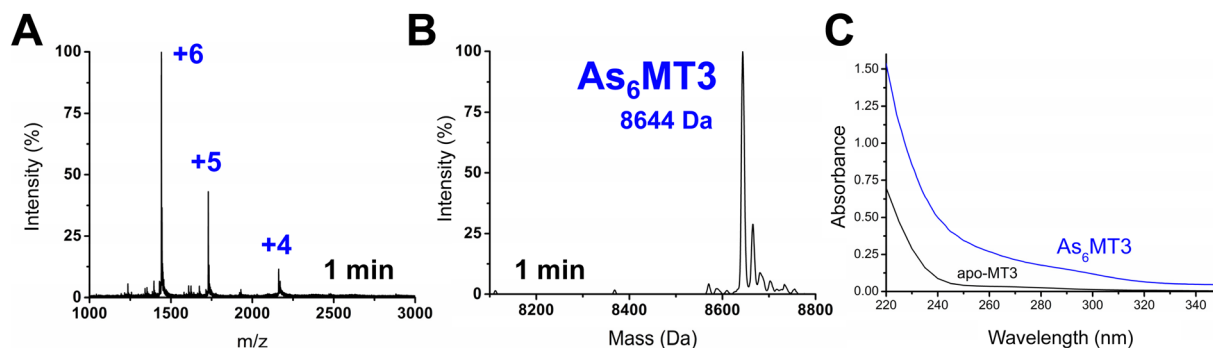


Fig. 2 As^{3+} metalation of apo-MT3 at pH 7.4, monitored using ESI-MS. The concentration of apo-MT3 used was $50 \mu\text{M}$ and 8 molar equivalents of As^{3+} from As_2O_3 were added. (A) Charge state spectrum at 1 minute post metalation. (B) Deconvoluted spectrum 1 minute post metalation. (C) UV-visible absorption spectrum of apo-MT3 and $\text{As}_6\text{MT3}$. The $\text{As}_6\text{MT3}$ was confirmed to be the sole species using ESI-MS.

The mass spectral data show that there is only one species in solution, $\text{As}_6\text{MT3}$ at a mass of 8644 Da, even though 8 molar equivalents of As^{3+} were added to the solution. The As^{3+} are likely coordinated with 3 cysteinyl thiols each, with no evidence of no bridging cysteines.⁵⁷ Any remaining cysteines are reduced as no disulfide bonds were noted by a 280 nm absorption band. This is comparable to the data illustrating As^{3+} binding to MT1.⁵⁷ Further support of the non-bridging noncooperative binding pathway was reported for MT1 in the past by linking three α domains together to form $\alpha\alpha\alpha$ -MT1, where there were 33

cysteine sites available.⁶⁷ In this case, only 11 As^{3+} bound to the protein, likely with each As^{3+} coordinated by 3 cysteinyl thiols.⁶⁷ This coordination is also consistent with that of trialkyl tri-thioarsenite compounds, $\text{As}(\text{SR})_3$, and $\text{As}(\text{GS})_3$ where trigonal-pyramidal geometry has been reported.^{68–73}

The absorption spectrum of the $\text{As}_6\text{MT3}$ solution shows a band at 290 nm (Fig. 2C). This band is relatively weak and has low molar absorptivity compared to the S–Cd charge transfer band. We identify 290 nm as the S–As charge-transfer band for

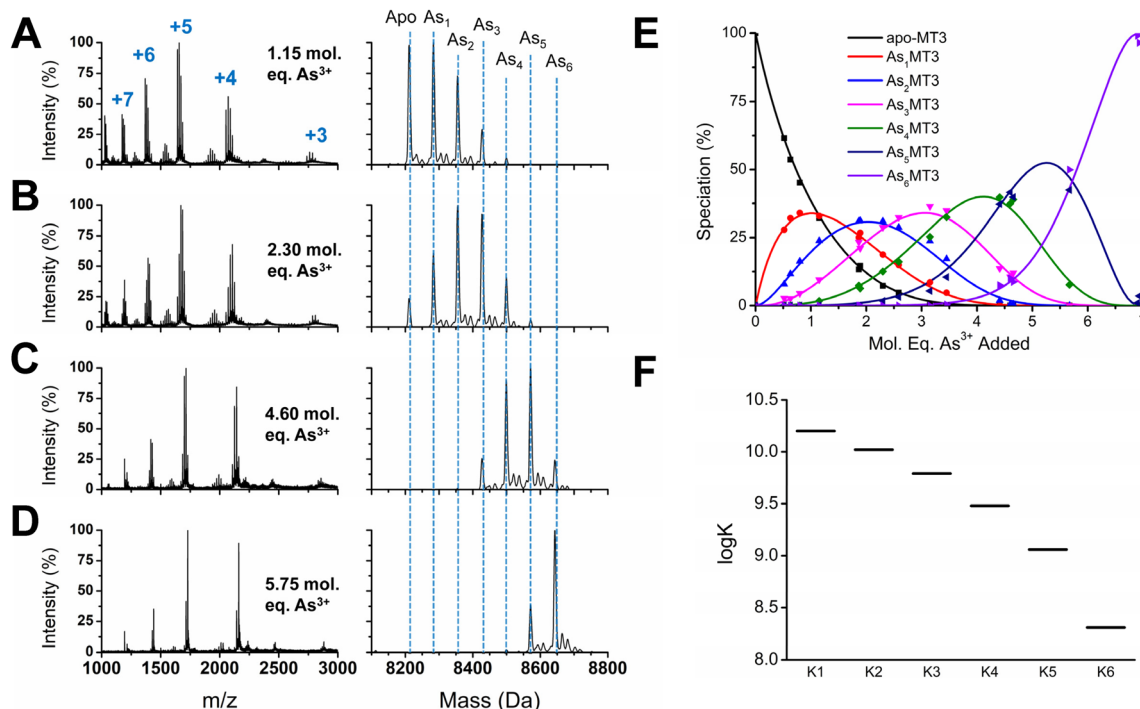
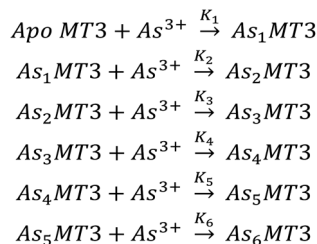
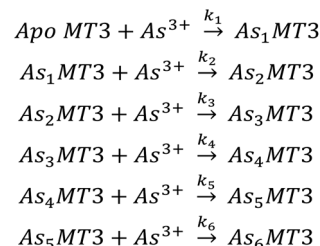


Fig. 3 As^{3+} stepwise titration into apo-MT3 with 3 molar equivalents of reduced GSH at pH 7.4. A sample of charge state spectra (left panels) and deconvoluted spectra (right panels) for As^{3+} added at 1.15 (A), 2.30 (B), 4.60 (C), and 5.75 (D) molar equivalents. All spectra were recorded for 2 minutes at ambient temperature. (E) Speciation of $\text{As}_n\text{MT3}$ species as a function of mol. eq. As^{3+} added to apo-MT3 in solution with GSH at pH 7.4. Symbols represent experimental data and solid lines represent model fitted to data. The model was calculated using HySS software. (F) Corresponding $\log K$ inputted to HySS. The $\log K$ values determined for each As^{3+} binding event are as follows: 10.20, 10.02, 9.79, 9.48, 9.06, and 8.31 M^{-1} .





Scheme 1 The sequential binding pathway for As^{3+} binding to apo-MT3. The equilibrium constants for each step are indicated by K_{1-6} for each As^{3+} binding event.



Scheme 2 The sequential binding pathway for As^{3+} binding to apo-MT3. The biomolecular rate constants for each step are indicated by k_{1-6} for each As^{3+} binding event.

MT3, similar to the previously reported 270 nm S-As charge-transfer band for $\text{As}(\text{GS})_3$.⁷⁴

Fig. 2 shows that at physiological pH, As^{3+} intermediates cannot be isolated due to the rapid binding of As^{3+} under these conditions. Stopped flow methods were considered for further analysis of the rate of As^{3+} binding to the apo-MT3, however, stopped flow data only provides an average rate constant

dependant on the absorption at the 290 nm charge transfer band. The implication of rapid binding of As^{3+} to apo-MT3 indicates potential dangers in arsenic poisoning, as it is not hindered kinetically from binding to apo-MTs at physiological pH; this is in contrast to the slow rates observed under acidic conditions.⁵⁷ This rapid binding of As^{3+} to apo-MT3 is similar to that observed in the early stages of Zn^{2+} and Cd^{2+} binding to

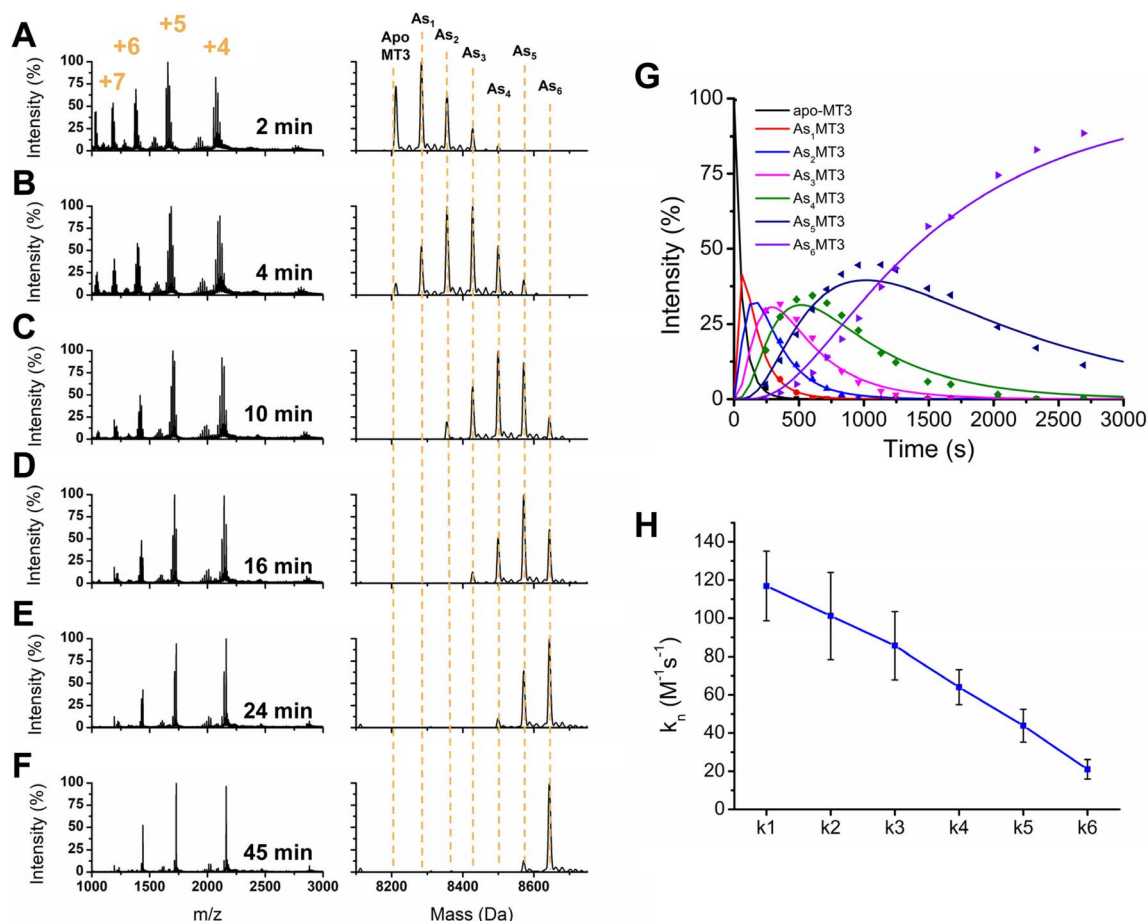


Fig. 4 As^{3+} binding to apo-MT3 as a function of time. 8 molar equivalents of As^{3+} were added to 20 μM apo-MT3 at pH 3.5. A total of 6 replicates were analyzed to ensure accuracy. (A–F) Charge state (left) and deconvoluted (right) mass spectra of As^{3+} metalation kinetics taken at 2 minutes (A), 4 minutes (B), 10 minutes (C), 16 minutes (D), 24 minutes (E), and 45 minutes (F) as a sample of data collected. Charge states are labelled on the first spectra and apply to the spectra below. Apo-MT3 and $\text{As}_n\text{MT3}$ species are labelled and applies to all spectra. (G) Speciation of $\text{As}_n\text{MT3}$ species as a function of time, with experimentally determined data represented by points and modelled speciation curves fitted by COPASI as solid lines. (H) Fitted rate constants for each As^{3+} binding event to MT3, with standard error represented by error bars.



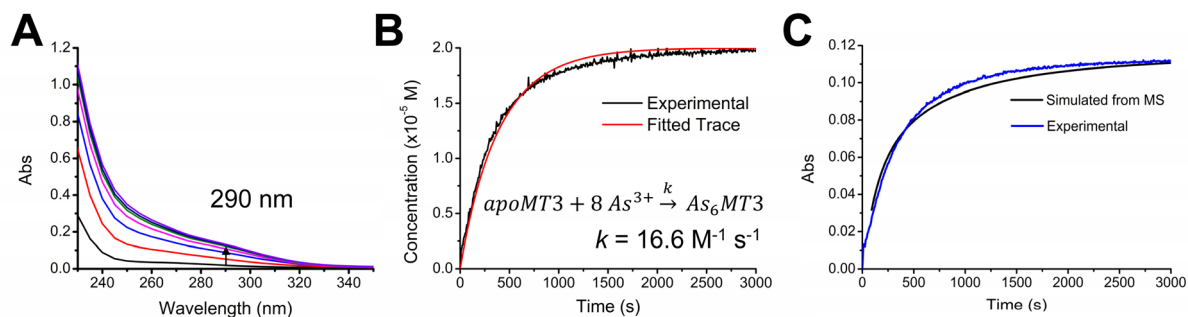


Fig. 5 As^{3+} binding to apo-MT3 at pH 3.5 monitored at 290 nm as a function of time. (A) Sample of absorption spectra taken at various time point intervals during the reaction. The arrow shows the 290 nm absorption band increasing in intensity as As^{3+} binds to apo-MT3. (B) Kinetic trace of As^{3+} binding determined by the 290 nm band (black line) and fitted trace determined by COPASI (red line). The fitted $k = 16.6 M^{-1} s^{-1}$. (C) Kinetic trace of As^{3+} binding experimentally determined by UV-visible spectroscopy (blue line) compared with the time-dependence of As^{3+} binding calculated from mass spectral data (black line).

apo-MTs, when the non-clustered terminally coordinated beads form.⁶⁵ However, to obtain more information on the partially metalated As-MT3 intermediates that form, we used stepwise As^{3+} metalation.

To determine the absolute binding constants for As^{3+} binding to apo-MT3 at pH 7.4, we used a competitive ligand with a known binding constant in solution with apo-MT3 (Fig. 3). In our case, we used the peptide glutathione (GSH), which binds to As^{3+} similarly to MT3 with a trigonal-pyramidal coordination with 3 molar equivalents of glutathione per As^{3+} ion.^{70,74,75} The reported binding constant for the $As(GS)_3$ complex is $\log \beta = 7$, therefore, this value was used in modelling the experimental data of binding of As^{3+} to apo-MT3 and GSH.⁷⁴ A sample of the ESI-mass spectral data collected (Fig. 3A–D) as well as speciation (Fig. 3E) and modelling data (Fig. 3F) are shown in Fig. 3.⁷⁶ The absolute binding constants ($\log K_n$, $n = 1-6$) for each As^{3+} binding step (Scheme 1) were determined: 10.20, 10.02, 9.79, 9.48, 9.06, and $8.31 M^{-1}$. Simulated mass spectra are generated using this model and compared to experimental spectra in ESI Fig. S1.† In addition, the first binding site was confirmed to be reasonable with the chelate effect equation: $\log K(\text{polydentate}) = \log \beta_n(\text{unidentate}) + (n - 1) \log 55.5$ where $\log K(\text{polydentate})$ is the binding constant of a n -dentate polydentate ligand (MT3, in this case) and $\log \beta_n(\text{unidentate})$ is the binding constant of the complex with n unidentate analogues (GSH) and 55.5 is the molarity of water, first described by Hancock *et al.*⁷⁷

To rule out protein–protein interactions, apo-MT3 in the absence of GSH was metalated with increasing molar equivalents of As^{3+} at pH 7.4 (Fig. S2†). The metalation profile shown in Fig. S1† is similar to that reported for MT1 metalated by As^{3+} under acidic pH conditions. For both proteins, we see noncooperative binding, or a normal distribution among As_nMT3 ($n = 1-6$) species centered on the average As^{3+} bound.⁶⁵ This means that there are no As_nMT3 species that are thermodynamically favoured or more stable than the rest. From the speciation diagram calculated from the raw data, we can model this stepwise titration with HySS software.⁷⁶ The same binding constants ($\log K_n$, $n = 1-6$) as determined above with GSH acting as

a competitive ligand can be fit to the experimental data (Fig. S3†).

We report that the metalation data recorded for As^{3+} binding to apo-MT3 in the presence and absence of GSH are essentially identical, as noted by the speciation diagrams shown in Fig. 3E and S3A.† This indicates that the presence of the competing GSH in solution with the apo-MT3 did not introduce additional interactions between the protein and the peptide, and thus, did not change the metalation pathway. We note that GSH does not effectively compete for the As^{3+} until MT3 has reached saturation. This is confirmed using the $\log K$ values for As^{3+} binding to MT3 and noting the free As^{3+} at an arbitrary point and comparing it to what was calculated for As^{3+} binding to GSH (Table S1†).

The binding constants obtained through this competition experiment are in the range of $\log K = 8-10$, which is surprisingly low compared with those of Zn^{2+} and Cd^{2+} . For Zn^{2+} , the $\log K$ values for each individual metalation step ranges from $\log K = 11-12$, whereas for Cd^{2+} , the values range from $\log K = 14-15$ for 7 binding steps. Since we see As^{3+} binding to apo-MT1 at pH 3.5, a condition that does not allow Cd^{2+} or Zn^{2+} binding as the protons outcompete the metal ions for the cysteinyl thiolates, we expected that the binding constants would be higher for As^{3+} binding. However, larger $\log K$ values do not accurately fit the As^{3+} binding data and the possibility of cluster formation and tetrahedral coordination may also further stabilize Zn^{2+} and Cd^{2+} bound MTs, and thus, resulting in a higher binding constant.²²

The binding constants for each subsequent As^{3+} binding event decrease, which is as a result of the statistical loss of available free thiols as the protein is sequentially metalated. This means that the last As^{3+} bound shows the least affinity, and therefore, may be outcompeted by other metals in the solution.

Because the pathway is noncooperative, As^{3+} can bind to apo-MT3 resulting in partially metalated As-MT3 species even with just one As^{3+} bound. In this manner the As^{3+} binding is similar to the initial stages of Zn^{2+} and Cd^{2+} binding, in which terminal thiolate coordination dominates. This property of As^{3+} binding also implies that partially metalated As-MT3 species are stable in solution, therefore, may not release As^{3+} into the cellular



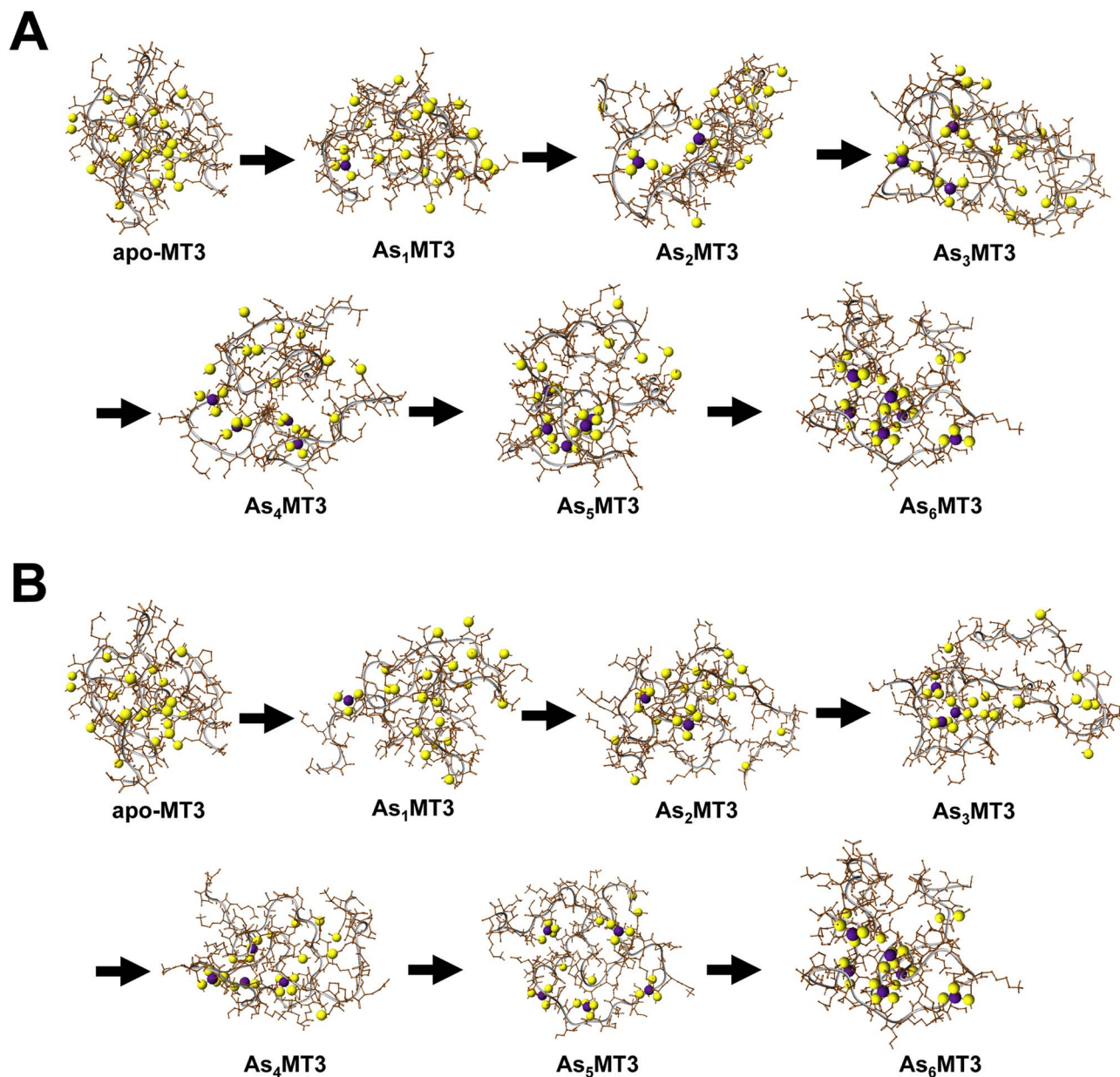


Fig. 6 Ribbon and ball-and-stick molecular models of representative As-MT3 species. The energy-minimized structures were calculated for 300 K conditions for 1000 ps with 0.02 ps equilibration time. The protein backbone is represented by the grey ribbon, the S atoms in yellow, the As³⁺ ions in purple, and the rest of the protein in brown. (A) The As³⁺ was bound to three cysteinyl thiolates sequentially starting at the N-terminal β domain (Cys1–3, Cys4–6, Cys7–9, Cys10–12, Cys13–15, Cys18–20), with the last As³⁺ bound by the last three thiolates due to the sequential thiolates occurring on either side of the acidic loop of the α domain. (B) The As³⁺ was bound to three cysteinyl thiolates sequentially starting at the C-terminal α domain, in reverse order to (A).

environment. Even though As³⁺ binding to MT3 shows decreased affinity after each subsequent binding event, the overall affinity of each of these reactions is relatively high and greater than the As³⁺ binding constant to glutathione as a result of the effect of multiple cysteines and the chelate effect.^{67,74} As MTs contain 20× the thiols of glutathione, the overall log β is much greater even though each As³⁺ involves 3 thiolates from the MT3 similar to the As(GS)₃ structure.

The trend in Fig. 3F shows that the log K values do not linearly decrease, suggesting the presence of additional factors

that impact As³⁺ binding. One possible reason for this non-linear trend is the rearrangement of bound As³⁺ in existing MT3 sites to accommodate the incoming As³⁺. Because of the trigonal pyramidal coordination with no evidence of bridging cysteines, As³⁺ binding thiolates are likely arranged in sequential order, therefore, if the first As³⁺ ions bound do not follow this pattern, rearrangement is necessary to bind the 6 As³⁺ ions that use the 18 cysteinyl thiolates.

With reference to the charge states in Fig. 3A–D, we note that the distribution of charge states for each spectrum as a function



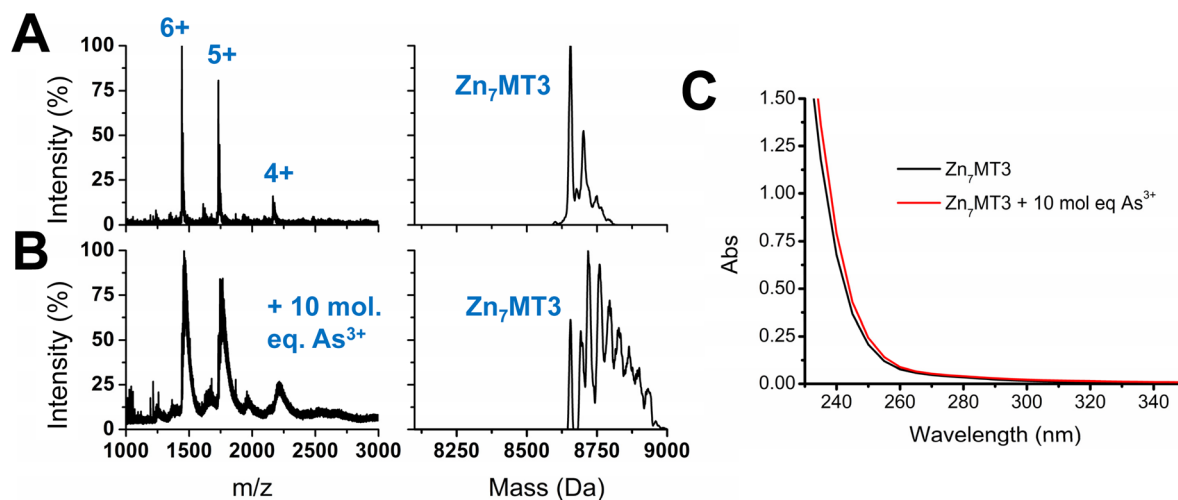


Fig. 7 As³⁺ binding to Zn₇MT3 at pH 7.4. (A and B) Charge state (left) and deconvoluted (right) spectra of Zn₇MT3 (A) and Zn₇MT3 with 10 molar equivalents of As³⁺ added (B). The charge states are labelled in the first panel and apply to the charge state spectrum below. The mass of Zn₇MT3 is labelled in the deconvoluted spectra. (C) Absorption spectra of Zn₇MT3 (black line) and Zn₇MT3 with 10 molar equivalents of As³⁺ added after 12 hours of reaction time.

of As³⁺ metal loading shifts to that of a lower weighted mean. For example, we see that the initial As³⁺ loading of MT3 (Fig. 3A) has charge states of mostly 5+ and 6+ with some 7+ and 4+, whereas As₃MT3 and As₆MT3 (Fig. 3D) has charge states of mostly 5+ and 4+ species. When looking at the weighted mean of the charge state present in the spectra, the value is +5.4 for apo-MT3, 4.8+ for As₆MT3, and 4.9+ for Cd₇MT3 (unpublished data). We note that the average weighted charge states for all these species are relatively similar, with apo-MT3 only slightly

larger, indicating a larger surface area.⁷⁸ This is mostly consistent with As-MT1 species, however, at physiological pH, we see that 5+ instead of 6+ is the dominant species.⁶⁵ This means that for MT3 under physiological conditions, we may see a greater percentage of more compact structures than we see for MT1 at pH 3. In comparison to Cd₇MT species, the 5+ charge state is similarly favoured under fully metalated conditions at physiological pH.^{22,79} From a structural point of view, it is clear that the two-cluster domains of Cd₇MT3 is likely as compact as the MT3

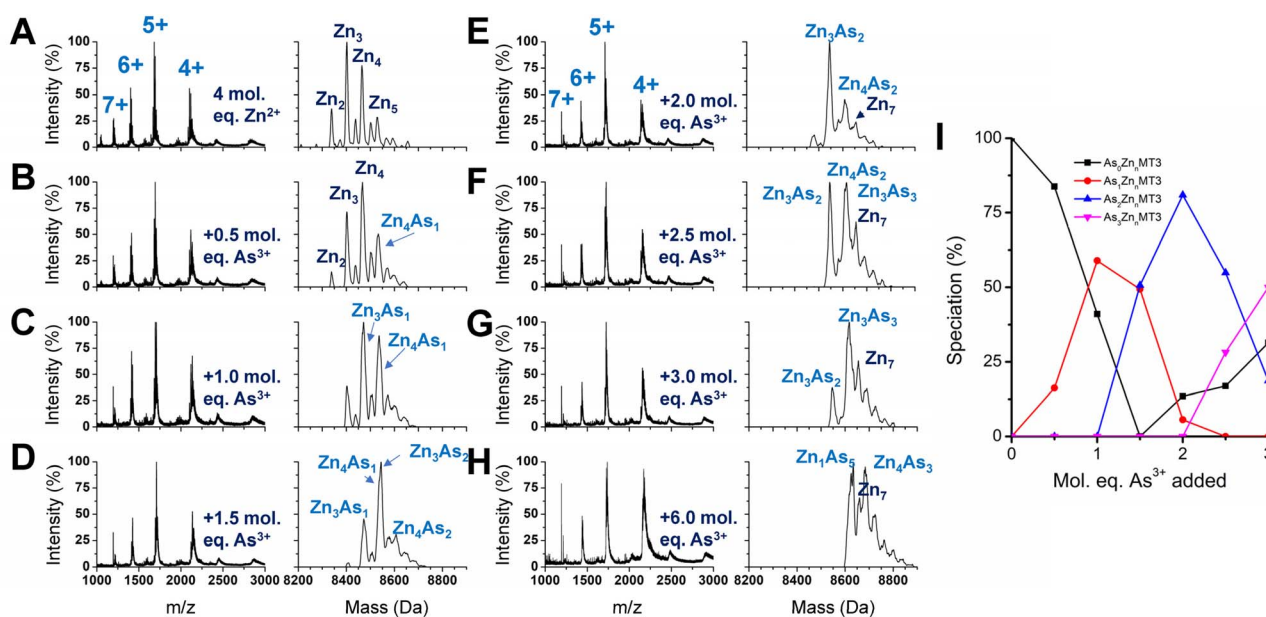


Fig. 8 As³⁺ titration into partially metalated Zn-MT3 at pH 7.4. (A–H) Charge state (left) and deconvoluted (right) spectra of As³⁺ added to the Zn-MT3 solution formed by adding 4 molar equivalents of Zn²⁺ to apo-MT3 with As³⁺ molar ratios of 0 molar equivalents (A), 0.5 molar equivalents (B), 1.0 molar equivalents (C), 1.5 molar equivalents (D) 2.0 molar equivalents (E), 2.5 molar equivalents (F), 3.0 molar equivalents (G), and 6.0 molar equivalents (H). (I) Speciation diagram of As_nMT3 species as a function of molar equivalents of As³⁺ added to the Zn-MT3 solution formed by adding 4 molar equivalents of Zn²⁺ to apo-MT3.



can be. However, it is evident from the data presented here that the $\text{As}_6\text{MT3}$ comprises 6 terminally coordinated As^{3+} that we associated with the term “beads” is also compact, which suggests that MTs generally adopt structures that limit exposure of the coordinating cysteines to the solvent. Our molecular dynamics calculations described below illustrate how compact the fully As-bound MT3 is (*vide infra* Fig. 6).

In addition, the elucidation of the binding mechanism of As^{3+} under physiological conditions further supports the mechanism of binding under acidic conditions as previously determined.⁵⁷ The kinetic parameters, as well as the thermal stability measurements, reported previously at pH 3.5 for MT1 may therefore be applicable in relative terms to the physiological pathway. This is surprising in some regard because of the changes in binding pathways seen for most other metals binding to MTs, for example, Bi^{3+} binds cooperatively at physiological pH but not under acidic conditions, and Zn^{2+} initially binds cooperatively under acidic conditions to form clusters but not under physiological conditions, where beads predominate initially.^{55,61}

The $\log K_n$ values for As^{3+} binding to apo-MT3 under physiological conditions reported here are especially important in the context of MT3 because MT3 is constitutively expressed and not metal-inducible. Therefore, it follows that the *de novo* apo-MT3 exists in cellular systems without Zn^{2+} protection at certain time points and is susceptible to As^{3+} binding in the event that As^{3+} is transported into the neural environment.

As^{3+} reaction rate when binding to apo-MT3 is faster than previously reported for apo-MT1

To further elucidate the As^{3+} binding pathway, we measured the As^{3+} binding kinetics using acidic pH to slow down the reaction. Each of the $\text{As}_n\text{MT3}$ ($n = 0-6$) species were observed *via* ESI-mass spectral data as a function of time (Fig. 4). Fig. 4A-F show a reduced selection of charge state spectra on the left panels and corresponding deconvoluted spectra on the right for different time points during the reaction. Fig. 4G shows the experimental points and corresponding fitted speciation as determined by COPASI using the Scheme 2 set of equations. The corresponding fitted bimolecular rate constants are plotted in Fig. 4H with error bars representing the standard deviation from the fitting of 6 separate experimental replicates. Each step of the As^{3+} metalation of apo-MT3 follows the second order reaction with the rate law: $\text{Rate} = k_n[\text{As}_{n-1}\text{MT3}][\text{As}^{3+}]$. The bimolecular rate constants determined for each As^{3+} binding to apo-MT3 at pH 3.5 are as follows: 116.9, 101.2, 85.6, 64.0, 43.9, and 21.0 $\text{M}^{-1} \text{s}^{-1}$.

One observation we can make about the kinetic data is that the trend in each stepwise rate constant is approximately linear (Fig. 4H). It follows that as the thiolate sites are used up for sequential As^{3+} binding that the rate decreases due to the lack of accessibility for subsequent binding. This is similar to the result noted for MT1.^{57,65} However, MT3 differs from MT1 in terms of the relation between k_1 and k_2 . For MT1, both the full protein and the α domain fragment exhibited a reduction in the magnitude of k_1 with respect to k_2 , which suggested that the first

As^{3+} was binding in the alpha domain region. For MT3, the rate constants of k_1 with respect to k_2 show the opposite pattern. This may be due to the α domain region being significantly different in structure because of the acidic loop insert that is located before the final three cysteines (Fig. 1). Another possible explanation for the absence of this inhibited first As^{3+} binding event is the fluxionality of the β domain of MT3, as suggested by Wang *et al.*⁵² Although the structure is compact, if the first binding site is located in the β domain, then As^{3+} may be able to access the thiols of that domain without significant interactions that reduce the rate.

Another observation we can make about the data is the similar shift of charge states as seen for the stepwise addition of As^{3+} under physiological conditions. Interestingly, the 5+ charge state remains the dominant species of $\text{As}_6\text{MT3}$ even at pH 3.5. This is indicative that the compact structure persists despite the expectation that at the acidic pH, the structure of MT3 would be more greatly expanded, and thus, would reveal higher charge states. We can also compare these data to those for MT1, where the 6+ charge state is the dominant species, indicating that MT3 is more compact when fully metalated.⁶⁰ This could have implications in the stability of the $\text{As}_6\text{MT3}$ as a possible protective mechanism against brain located As^{3+} species.

Lastly, the data in Fig. 4 show that the rate constants for As^{3+} binding at pH 3.5 are significantly faster than those measured for MT1. For MT1, the rate constant values ranged from 4–25 $\text{M}^{-1} \text{s}^{-1}$ at room temperature.⁶⁵ This is already significantly faster than observed for the single domain fragments, which ranged from 1–7 $\text{M}^{-1} \text{s}^{-1}$ for both the β and α domains.⁵⁷ In contrast, the rate constants for MT3 range from 20 to 117 $\text{M}^{-1} \text{s}^{-1}$. Considering the similarity between the sequence and available cysteines of apo-MT3 and apo-MT1, this is surprising.

However, there is a major difference in the structural positioning of the final 3 cysteines in MT3 compared with MT1. Based on the analysis of Ngu *et al.* that the first As^{3+} bound in α domain, we can consider whether the last 3 cysteines are significantly more exposed to the solvent and therefore allow more rapid binding. The rate of the first As^{3+} bound controls the subsequent 5 reactions. Ngu *et al.* suggested that the evolution of a two-domain structure of MT1 was important in that the probability of collision with correct orientation between the thiols and As^{3+} was increased as a function of the number of thiols in the protein, thus, providing evidence for its efficacy as a metal scavenger.⁶⁵ In MT3, we now see also that the availability of those thiols can change the rate of reaction, where in this case the acidic loop changes the overall structure of the protein.

To introduce a secondary source of kinetic data, we monitored the As^{3+} binding mechanism using UV-visible spectroscopy and compared the overall rate determined with the ESI-mass spectral data under the same conditions (Fig. 5). We used the 290 nm S-As charge transfer band as an indicator of As^{3+} binding and determined an overall rate constant of 16.6 $\text{M}^{-1} \text{s}^{-1}$. Using ESI-MS data outlined in Fig. 4, we can determine the average As^{3+} bound to MT3 as a function of time and plot it against the kinetic trace determined using UV-visible spectroscopy (Fig. 5C). these data confirm that the mass spectral data



are correlated with the solution reactions obtained from the absorption spectroscopy, and that the overall kinetic parameters determined from ESI-mass spectral data can be reliably used in the case of As^{3+} binding to MT3.

Modelling the structure of $\text{As}_n\text{MT3}$ ($n = 0-6$)

The structures of the As^{3+} bound to apo-MT3 can be modelled using Scigress Modelling Software (Fig. 6). There are two steps in this calculation: the first being the molecular mechanics minimization of the structure as constructed and the second being the use of molecular dynamics to search for the lowest energy structure. The conditions used in the molecular dynamics step were 300 K and the calculation was performed for 1000 ps with 0.02 ps equilibration time to select for the energy-minimized structure of each $\text{As}_n\text{MT3}$ structure. We showed As^{3+} sequential metalation both starting in the N-terminal β domain (Fig. 6A) and C-terminal α domain (Fig. 6B).

The series of structures in Fig. 6 show that binding As^{3+} does not significantly change the overall surface area of MT3. This is confirmed using solvent accessible surface area (SASA) calculations, where all structures show SASAs of 5500–6300 \AA^2 .⁸¹ As an apoprotein, MT3 is still relatively compact, as determined previously.⁸⁰ The addition of As^{3+} to the MT3 does not result in a specific structure when compared, for example, to the structure of Zn_7MT with its two cluster domains. The As^{3+} bound to the protein, however, is relatively shielded and located in the interior space of the protein. This may explain the minimal change to lower charge states upon metalation (Fig. 3 and 4).⁷⁸ Our models also demonstrate that since the structure of MT3 is not greatly impacted by metalation, the subsequent As^{3+} binding sites are not significantly different or shielded, therefore explaining the linearly decreasing rate constants of As^{3+} binding attributed to the decreasing availability of sites illustrated in Fig. 4.

As^{3+} does not outcompete fully metalated $\text{Zn}_7\text{MT3}$

With the knowledge of the binding constants of As^{3+} binding to apo-MT3 as well as the binding pathway involved in the metalation process, we further extended our work to include $\text{Zn}_7\text{MT3}$, which is fully metalated with no cysteines available for binding additional metals. Essentially, we were interested in determining whether As^{3+} would be able to displace Zn^{2+} in MT3 under physiological pH, as it could further provide information on the conditions under which As^{3+} could be disruptive to the functions of MT3. The results obtained by the addition of 10 molar equivalents of As^{3+} to $\text{Zn}_7\text{MT3}$ at pH 7.4 are summarized in Fig. 7. ESI-mass spectral data show the continued presence of $\text{Zn}_7\text{MT3}$ before the reaction and the changes in the spectrum obtained after As^{3+} addition can be attributed to adduct formation (Fig. 7A and B). This reaction can be further analyzed using UV-visible spectroscopy, where we note the minimal change in absorption after the addition of As^{3+} even after 12 hours of reaction time (Fig. 7C). Our interpretation is that the As^{3+} added does not displace Zn^{2+} , as the absorption that we noted for the S-As charge transfer band at 290 nm does not appear in Fig. 7C.

This result can be explained by the lower binding constants obtained for As^{3+} metalation of apo-MT3, as it was in the range of $\log K = 8-10$, which, for the first As^{3+} bound, would be an order of magnitude lower than that of Zn^{2+} binding, which is in the range of $\log K = 11-12$.

For $\text{Zn}_7\text{MT3}$, the Zn^{2+} is coordinated by bridging cysteines to form stable Zn_4S_{11} and Zn_3S_9 clusters in the α and β domains, respectively.²² These clusters are formed cooperatively at low pH and in the presence of over 5 molar equivalents of Zn^{2+} .^{22,61,82} Interestingly, it has been suggested that the clusters of the individual domains of MT3 may be less stable compared with those of the other MT isoforms. This is illustrated by pH-induced unfolding, where fully metalated MT2 shows a two step unfolding process for each domain in comparison to the absent two step distinction for metalated MT3.⁸³ In addition, ¹¹³Cd NMR studies show minor resonances for the ¹¹³Cd bound to the β domain compared to that of the α domain and ¹⁵N NMR studies illustrate the fluxionality of the β domain, suggesting the instability of this domain in comparison to other MT isoforms.^{52,83} However, even with the fluxional structure of fully metalated $\text{Zn}_7\text{MT3}$, full metalation offers protection from As^{3+} metalation. Due to the coordination of the Zn^{2+} in fully metalated MT proteins, the As^{3+} would have to disrupt the clustered Zn_4S_{11} and Zn_3S_9 structures in order to bind in a noncooperative manner.

As^{3+} can change Zn^{2+} distribution in partially metalated Zn-MT3 species

We used partially metalated Zn-MT3 species as a starting point to better emulate physiological conditions when As^{3+} may bind to existing Zn-MT3 . We believe this is a better representation of how MT3 exists in the cellular environment because of the presence of additional MTs that can be induced by Zn^{2+} presence.^{22,82} Therefore, it is unlikely for MTs to be fully metalated at any point in time as it would further trigger the production of additional MT.

We chose to start with 4 molar equivalents of Zn^{2+} , which forms multiple species including $\text{Zn}_2\text{MT3}$, $\text{Zn}_3\text{MT3}$, $\text{Zn}_4\text{MT3}$, and $\text{Zn}_5\text{MT3}$ using terminal thiolates in the “bead” structural model (Fig. 8A). Adding even 0.5 molar equivalents of As^{3+} changes the distribution of Zn^{2+} species, meaning that the Zn^{2+} ions are able to rearrange (Fig. 8B). This is especially evident if we look at the ratio of $\text{Zn}_3\text{MT3}$ to $\text{Zn}_4\text{MT3}$, where $\text{Zn}_3\text{MT3}$ became less favored as a species in solution with the addition of As^{3+} , even with the $\text{Zn}_4\text{MT3}$ species forming mixed As^{3+} species ($\text{Zn}_4\text{As}_1\text{MT3}$). Adding more As^{3+} molar equivalents to the solution results in additional rearrangement of Zn^{2+} with predominantly Zn_3 and Zn_4 species existing as mixed Zn,As-MT3 species in solution (Fig. 8B–H). However, due to the overlap in masses of mixed Zn,As-MT3 species, not all peaks were identified. However, of the identified peaks, it is important to note the prevalence of Zn_4As_3 species, which we believe is representative of 4 Zn^{2+} coordinated by the α domain of the protein in the classic cluster conformation and 3 As^{3+} terminally coordinated by the 9 cysteines of the β domain. Therefore, in the presence of Zn^{2+} , we speculate



that As^{3+} preferentially binds to the N-terminal β domain in MT3. We note that this is contrary to our interpretation of the binding pathway for apo-MT3 above and suggests that the presence of Zn^{2+} in MT3 may significantly influence the binding of xenobiotic metals by forming substitution-resistant clusters in the α domain.

If we look specifically at the As^{3+} bound MT3 and track the number of As^{3+} bound as a function of As^{3+} added, it is similar to the As^{3+} titration at pH 7.4, where As^{3+} binds sequentially (Fig. 8I). This means that all sites for As^{3+} binding in partially metalated Zn-MT3 are similar to sites in apo-MT3 – the partial metalation with Zn^{2+} does not impede additional As^{3+} binding significantly until the As_5 point associated with $\text{Zn}_1\text{As}_5\text{MT3}$.

We note that the binding constants of As^{3+} binding to MT3 are lower than the comparable binding constants for Zn^{2+} binding to MT3. It appears that when As^{3+} binds to partially metalated Zn-MT3, the species that form maximize the use of 20 cysteines so that $\text{Zn}_1\text{As}_5\text{MT3}$ forms, using 19 cysteines, and $\text{Zn}_4\text{As}_3\text{MT3}$ forms, using 20 cysteines, and $\text{Zn}_7\text{MT3}$ using 20 cysteines forms. This indicates that the metals bound in MT3 rearrange to maximize the number of cysteines involved in the structures. What this suggests is that because mammalian MTs are not considered to be fully metalated under normal conditions, xenobiotic metals such as As^{3+} , Bi^{3+} and Pt^{2+} can take advantage of the cysteine availability to form mixed-metal structures with no displacement being required of the existing Zn^{2+} .

This experiment with partially metalated Zn-MT3 further probes the properties of As^{3+} binding under physiological conditions, where MT3 may not be fully protected as a fully metalated $\text{Zn}_7\text{MT3}$ protein, but instead exists as multiple partially metalated species. This may imply that Zn^{2+} supplementation could be beneficial to As^{3+} poisoning and Zn^{2+} deficiency exacerbates As^{3+} poisoning effects, which has been suggested in the past in rat and mouse model systems.^{3,84–87}

Conclusions

Arsenic poisoning has long been a reoccurring problem worldwide due to water contamination. Amongst the effects of arsenic poisoning are neurological issues, thus, it is important to study the brain-located metallochaperone, MT3. This paper reports novel information regarding As^{3+} binding to MT3, including absolute binding constants of each individual As^{3+} to apo-MT3 under physiological conditions, as well as ESI-mass spectral data of fast As^{3+} binding to apo-MT3 at pH 7.4. In addition, we have provided evidence that the binding pathway determined kinetically at pH 3.5 follows the binding pathway determined with stepwise metalation at pH 7.4. There appears to be no specific pH dependence in binding pathway for MT3. In addition, we have shown that fully metalated $\text{Zn}_7\text{MT3}$ impedes As^{3+} binding at pH 7.4, but partial metalation with Zn^{2+} does not significantly impact As^{3+} binding. This provides support that Zn^{2+} supplementation will be protective against As^{3+} poisoning of MTs.

Data availability

All experimental details and data supporting the findings of this study are available in the paper and in the ESI.† Any additional data are available from the corresponding author upon request.

Author contributions

A. T. Y. and M. J. S. designed the experiments and conceived the project. A. T. Y. carried out the experiments and analysis with the guidance of M. J. S. All authors contributed to the manuscript.

Conflicts of interest

There are no conflicts to declare.

Acknowledgements

We thank the Natural Sciences and Engineering Research Council of Canada for a Canada Graduate Scholarship Doctoral (CGS-D) to A. T. Y. and a Discovery Grant (06545-2020) to M. J. S. We would like to thank Mr John Vanstone, Ms Melanie Glover, and Mr Barakat Misk of the Electronics Shop at the University of Western Ontario for the outstanding maintenance of our instruments.

References

- 1 IARC, *Arsenic, Metals, Fibres, and Dusts*, International Agency for Research on Cancer, Lyon, France, 2012.
- 2 S. Rahman, K.-H. Kim, S. K. Saha, A. M. Swaraz and D. K. Paul, *J. Environ. Manage.*, 2014, **134**, 175–185.
- 3 Q. Y. Chen and M. Costa, *Annu. Rev. Pharmacol. Toxicol.*, 2021, **61**, 47–63.
- 4 J. Y. Chung, S. D. Yu and Y. S. Hong, *J. Prev. Med. Public Health*, 2014, **47**, 253–257.
- 5 S. Shen, X.-F. Li, W. R. Cullen, M. Weinfeld and X. C. Le, *Chem. Rev.*, 2013, **113**, 7769–7792.
- 6 Y. Y. Chang, T. C. Kuo, C. H. Hsu, D. R. Hou, Y. H. Kao and R. N. Huang, *Arch. Toxicol.*, 2012, **86**, 911–922.
- 7 A. Vahidnia, G. B. van der Voet and F. A. de Wolff, *Hum. Exp. Toxicol.*, 2007, **26**, 823–832.
- 8 R. K. Virk, R. Garla, N. Kaushal, M. P. Bansal, M. L. Garg and B. P. Mohanty, *Chemosphere*, 2023, **316**, 137735.
- 9 K. Rehman and H. Naranmandura, *Metallomics*, 2012, **4**, 881–892.
- 10 R. N. Ratnaike, *Postgrad. Med. J.*, 2003, **79**, 391.
- 11 G. A. Wasserman, X. Liu, F. Parvez, P. Factor-Litvak, H. Ahsan, D. Levy, J. Kline, A. van Geen, J. Mey, V. Slavkovich, A. B. Siddique, T. Islam and J. H. Graziano, *Neurotoxicology*, 2011, **32**, 450–457.
- 12 M. Tolins, M. Ruchirawat and P. Landrigan, *Ann. Glob. Health*, 2014, **80**, 303–314.
- 13 J. S. Tsuji, M. R. Garry, V. Perez and E. T. Chang, *Toxicology*, 2015, **337**, 91–107.
- 14 H. Mochizuki, *Int. J. Mol. Sci.*, 2019, **20**(14), 3418.



- 15 M. Thakur, M. Rachamalla, S. Niyogi, A. K. Datusalia and S. J. Flora, *Int. J. Mol. Sci.*, 2021, **22**(18), 10077.
- 16 L. P. Chandravanshi, R. Gupta and R. K. Shukla, *Biol. Trace Elem. Res.*, 2018, **186**, 185–198.
- 17 C. Prakash, M. Soni and V. Kumar, *J. Appl. Toxicol.*, 2016, **36**, 179–188.
- 18 P. Coyle, J. C. Philcox, L. C. Carey and A. M. Rofe, *Cell. Mol. Life Sci.*, 2002, **59**, 627–647.
- 19 P. Babula, M. Masarik, V. Adam, T. Eckschlager, M. Stiborova, L. Trnkova, H. Skutkova, I. Provaznik, J. Hubalek and R. Kizek, *Metallomics*, 2012, **4**, 739–750.
- 20 C. D. Klaassen, J. Liu and S. Choudhuri, *Annu. Rev. Pharmacol. Toxicol.*, 1999, **39**, 267–294.
- 21 M. Namdarghanbari, W. Wobig, S. Krezoski, N. M. Tabatabai and D. H. Petering, *J. Biol. Inorg. Chem.*, 2011, **16**, 1087.
- 22 D. E. K. Sutherland and M. J. Stillman, *Metallomics*, 2011, **3**, 444–463.
- 23 M. J. Stillman, *Coord. Chem. Rev.*, 1995, **144**, 461–511.
- 24 J. H. R. Kägi, S. R. Himmelhoch, P. D. Whanger, J. L. Bethune and B. L. Vallee, *J. Biol. Chem.*, 1974, **249**, 3537–3542.
- 25 A. Z. Mason, N. Perico, R. Moeller, K. Thrippleton, T. Potter and D. Lloyd, *Mar. Environ. Res.*, 2004, **58**, 371–375.
- 26 A. Z. Mason, R. Moeller, K. A. Thrippleton and D. Lloyd, *Anal. Biochem.*, 2007, **369**, 87–104.
- 27 T. B. Pinter and M. J. Stillman, *Biochemistry*, 2014, **53**, 6276–6285.
- 28 A. T. Yuan, N. C. Korkola, D. L. Wong and M. J. Stillman, *Metallomics*, 2020, **12**, 767–783.
- 29 M. Nakajima, E. Kobayashi, Y. Suwazono, M. Uetani, M. Oishi, T. Inaba, T. Kido, Z. A. Shaikh and K. Nogawa, *Biol. Trace Elem. Res.*, 2005, **108**, 17–31.
- 30 N. Sugawara, D. Li and C. Sugawara, *Arch. Toxicol.*, 1994, **68**, 520–523.
- 31 E. M. Kenyon, M. F. Hughes, B. M. Adair, J. H. Highfill, E. A. Crecelius, H. J. Clewell and J. W. Yager, *Toxicol. Appl. Pharmacol.*, 2008, **232**, 448–455.
- 32 M. S. Samuel, S. Datta, R. S. Khandge and E. Selvarajan, *Sci. Total Environ.*, 2021, **775**, 145829.
- 33 T. Miura, S. Muraoka and T. Ogiso, *Life Sci.*, 1997, **60**, 301–309.
- 34 K.-S. Min, F. Morishita, N. Tetsuchikawahara and S. Onosaka, *Toxicol. Appl. Pharmacol.*, 2005, **204**, 9–17.
- 35 W. Maret, *Neurochem. Int.*, 1995, **27**, 111–117.
- 36 T. Kimura and T. Kambe, *Int. J. Mol. Sci.*, 2016, **17**(3), 336.
- 37 M. Vašák and G. Meloni, *J. Biol. Inorg. Chem.*, 2011, **16**, 1067.
- 38 M. Vašák and D. W. Hasler, *Curr. Opin. Chem. Biol.*, 2000, **4**, 177–183.
- 39 A. T. Miles, G. M. Hawksworth, J. H. Beattie and V. Rodilla, *Crit. Rev. Biochem. Mol. Biol.*, 2000, **35**, 35–70.
- 40 I. Hozumi, J. S. Suzuki, H. Kanazawa, A. Hara, M. Saio, T. Inuzuka, S. Miyairi, A. Naganuma and C. Tohyama, *Neurosci. Lett.*, 2008, **438**, 54–58.
- 41 Y. Uchida, K. Takio, K. Titani, Y. Ihara and M. Tomonaga, *Neuron*, 1991, **7**, 337–347.
- 42 A. Krężel and W. Maret, *Chem. Rev.*, 2021, **121**, 14594–14648.
- 43 M. Vašák and G. Meloni, *Int. J. Mol. Sci.*, 2017, **18**, 1117.
- 44 G. Meloni, V. Sonois, T. Delaine, L. Guilloreau, A. Gillet, J. Teissié, P. Faller and M. Vašák, *Nat. Chem. Biol.*, 2008, **4**, 366–372.
- 45 Y. Manso, J. Carrasco, G. Comes, G. Meloni, P. A. Adlard, A. I. Bush, M. Vasak and J. Hidalgo, *Cell. Mol. Life Sci.*, 2012, **69**, 3683–3700.
- 46 A. Binolfi, G. R. Lamberto, R. Duran, L. Quintanar, C. W. Bertocini, J. M. Souza, C. Cerveñansky, M. Zweckstetter, C. Griesinger and C. O. Fernández, *J. Am. Chem. Soc.*, 2008, **130**, 11801–11812.
- 47 Y. Irie and W. M. Keung, *Brain Res.*, 2003, **960**, 228–234.
- 48 G. Meloni and M. Vašák, *Free Radic. Biol. Med.*, 2011, **50**, 1471–1479.
- 49 J. S. Calvo, N. V. Mulpuri, A. Dao, N. K. Qazi and G. Meloni, *Free Radic. Biol. Med.*, 2020, **158**, 149–161.
- 50 J. Y. Koh and S. J. Lee, *Mol. Brain*, 2020, **13**, 116.
- 51 Q. Zheng, W. M. Yang, W. H. Yu, B. Cai, X. C. Teng, Y. Xie, H. Z. Sun, M. J. Zhang and Z. X. Huang, *Protein Eng. Des. Sel.*, 2003, **16**, 865–870.
- 52 H. Wang, Q. Zhang, B. Cai, H. Li, K.-H. Sze, Z.-X. Huang, H.-M. Wu and H. Sun, *FEBS Lett.*, 2006, **580**, 795–800.
- 53 J. S. Scheller, G. W. Irvine, D. L. Wong, A. Hartwig and M. J. Stillman, *Metallomics*, 2017, **9**, 447–462.
- 54 A. Melenbacher, N. C. Korkola and M. J. Stillman, *Metallomics*, 2020, **12**, 1951–1964.
- 55 N. C. Korkola, P. M. Scarrow and M. J. Stillman, *Metallomics*, 2020, **12**, 435–448.
- 56 N. C. Korkola, E. Hudson and M. J. Stillman, *Metallomics*, 2021, **13**.
- 57 T. T. Ngu and M. J. Stillman, *J. Am. Chem. Soc.*, 2006, **128**, 12473–12483.
- 58 M. R. Mehlenbacher, R. Elsiesy, R. Lakha, R. L. E. Villones, M. Orman, C. L. Vizcarra, G. Meloni, D. E. Wilcox and R. N. Austin, *Chem. Sci.*, 2022, **13**, 5289–5304.
- 59 C. Pérez-Zúñiga, A. Leiva-Presa, R. N. Austin, M. Capdevila and O. Palacios, *Metallomics*, 2019, **11**, 349–361.
- 60 J. S. Calvo, R. L. E. Villones, N. J. York, E. Stefaniak, G. E. Hamilton, A. L. Stelling, W. Bal, B. S. Pierce and G. Meloni, *J. Am. Chem. Soc.*, 2022, **144**, 709–722.
- 61 G. W. Irvine, T. B. Pinter and M. J. Stillman, *Metallomics*, 2016, **8**, 71–81.
- 62 R. Garla, N. Kaur, M. P. Bansal, M. L. Garg and B. P. Mohanty, *J. Mol. Model.*, 2017, **23**, 78.
- 63 M. Toyama, M. Yamashita, N. Hirayama and Y. Murooka, *J. Biochem.*, 2002, **132**, 217–221.
- 64 Y. He and J. Guo, *Comput. Theor. Chem.*, 2015, **1058**, 54–60.
- 65 T. T. Ngu, A. Easton and M. J. Stillman, *J. Am. Chem. Soc.*, 2008, **130**, 17016–17028.
- 66 T. T. Ngu, S. Krecisz and M. J. Stillman, *Biochem. Biophys. Res. Commun.*, 2010, **396**, 206–212.
- 67 T. T. Ngu, J. A. Lee, T. B. Pinter and M. J. Stillman, *J. Inorg. Biochem.*, 2010, **104**, 232–244.
- 68 J.-H. Chou and M. G. Kanatzidis, *Inorg. Chem.*, 1994, **33**, 1001–1002.
- 69 B. T. Farrer, C. P. McClure, J. E. Penner-Hahn and V. L. Pecoraro, *Inorg. Chem.*, 2000, **39**, 5422–5423.



- 70 N. A. Rey, O. W. Howarth and E. C. Pereira-Maia, *J. Inorg. Biochem.*, 2004, **98**, 1151–1159.
- 71 K. Tani, S.-i. Hanabusa, S. Kato, S.-y. Mutoh, S.-i. Suzuki and M. Ishida, *J. Chem. Soc., Dalton Trans.*, 2001, 518–527, DOI: [10.1039/B008702P](https://doi.org/10.1039/B008702P).
- 72 G. C. Pappalardo, R. Chakravorty, K. J. Irgolic and E. A. Meyers, *Acta Crystallogr. C*, 1983, **39**, 1618–1620.
- 73 B. F. Hoskins, E. R. T. Tiekink and G. Winter, *Inorg. Chim. Acta*, 1985, **99**, 177–182.
- 74 A. M. Spuches, H. G. Kruszyna, A. M. Rich and D. E. Wilcox, *Inorg. Chem.*, 2005, **44**, 2964–2972.
- 75 N. Scott, K. M. Hatlelid, N. E. MacKenzie and D. E. Carter, *Chem. Res. Toxicol.*, 1993, **6**, 102–106.
- 76 L. Alderighi, P. Gans, A. Ienco, D. Peters, A. Sabatini and A. Vacca, *Coord. Chem. Rev.*, 1999, **184**, 311–318.
- 77 R. D. Hancock and A. E. Martell, *Chem. Rev.*, 1989, **89**, 1875–1914.
- 78 I. A. Kaltashov and A. Mohimen, *Anal. Chem.*, 2005, **77**, 5370–5379.
- 79 D. E. Sutherland and M. J. Stillman, *Biochem. Biophys. Res. Commun.*, 2008, **372**, 840–844.
- 80 A. T. Yuan, N. C. Korkola and M. J. Stillman, *J. Biol. Chem.*, 2023, **299**(3), 102899.
- 81 R. Fraczkiewicz and W. Braun, *J. Comput. Chem.*, 1998, **19**, 319–333.
- 82 D. E. K. Sutherland, K. L. Summers and M. J. Stillman, *Biochemistry*, 2012, **51**, 6690–6700.
- 83 D. W. Hasler, L. T. Jensen, O. Zerbe, D. R. Winge and M. Vašák, *Biochemistry*, 2000, **39**, 14567–14575.
- 84 R. Ganger, R. Garla, B. P. Mohanty, M. P. Bansal and M. L. Garg, *Biol. Trace Elem. Res.*, 2016, **169**, 218–229.
- 85 M. Ahmad, M. A. M. Wadaan, M. Farooq, M. H. Daghestani and A. S. Sami, *Biol. Res.*, 2013, **46**, 131–138.
- 86 C. P. Wong, E. J. Dashner-Titus, S. C. Alvarez, T. T. Chase, L. G. Hudson and E. Ho, *Biol. Trace Elem. Res.*, 2019, **191**, 370–381.
- 87 L. M. Beaver, L. Truong, C. L. Barton, T. T. Chase, G. D. Gonnerman, C. P. Wong, R. L. Tanguay and E. Ho, *PLoS One*, 2017, **12**, e0183831.

